Available online at www.sciencedirect.com
ScienceDirect
Thermochimica Acta 455 (2007) 34–39
thermochimica acta
www.elsevier.com/locate/tca

Estimations of local heat release rate in the methane–air premixed flames

G.-M. Choi [a,*], J.-S. Yang [b,1], D.-J. Kim [a,2], M. Tanahashi [c,3], T. Miyauchi [c,4]

[a] School of Mechanical Engineering, Pusan National University, 30 Jangjeon-dong, Geumjeoung-ku, Busan 609-735, Republic of Korea
[b] Research Institute of Mechanical Technology, Pusan National University, 30 Jangjeon-dong, Geumjeoung-ku, Busan 609-735, Republic of Korea
[c] Department of Mechanical and Aerospace Engineering, Tokyo Institute of Technology, 2-12-1 Ookayama, Meguro-ku, Tokyo 152-8552, Japan

Available online 28 November 2006

Abstract

Relationships between the local heat release rate and CH concentration have been investigated by numerical simulations of methane–air premixed flames and simultaneous CH and OH PLIF (planar laser-induced fluorescence) measurement has been also conducted for lean cellular premixed flame as well as for laminar flames. The distance between the peak of heat release rate and that of CH concentration is less than 91 μm for all equivalence ratios calculated. Even for the premixed flame in high intensity turbulence, the distribution of the heat release rate coincides with that of CH mole fraction. For CH PLIF measurements, CH fluorescence intensity in terms of equivalence ratio shows a similar trend with CH mole fraction computed by GRI mechanism even in lean conditions. These results imply that CH PLIF measurements can be applicable to the estimation of the spatial fluctuations of heat release rate in the turbulent premixed flame.

Keywords: Local heat release rate; CH concentration; Direct numerical simulation; Planar laser-induced fluorescence; Premixed flame

1. Introduction

Lean combustion is commonly used for low pollution and fuel saving in the combustion-driven energy systems. However, unsteady oscillation due to lean combustion often results in combustion noise as well as oscillatory combustion. Combustion noise is produced by the interaction between the vortex structures and flame in the shear flows. Effective control of oscillating flame, therefore, is strongly required for control of combustion-driven energy system.

In order to develop control scheme of the combustion, detail understandings of the flame structures in combustor is quite important. Owing to remarkable developments of the laser diagnostics in the combustion field, detailed structure of the turbulent flames can be measured by a particle image velocimetry (PIV), a planar laser-induced fluorescence (PLIF), etc. In order to study the properties of the flame surface experimentally, the location of the flame surface has to be determined accurately. The presence of CH proves that some main oxidation reaction is occurring, that is, a flame should exist at this region. As a marker for flame surface, CH PLIF have been used to investigate the flame fronts in turbulent flames because CH radicals are produced at the flame front and have very narrow width enough to represent the reaction zone [1,2]. Many research groups, therefore, have used the CH radical as a marker for reaction zone in the various flames [3–5]. Calculations in a laminar CH_4–N_2–air flame indicate that the OH peak mole fraction occurs in the burned side, whereas the CH peak is in the unburned side [6]. Thus, the location between CH and OH maximum region has been used as a marker of stoichiometric contour [3]. Although some reports [7,8] warned that CH concentration is not universally correlated with heat release rate and may wrongly indicate breaks in the flame surface, CH radical, which possibly represents most of reaction zone, can provide deep insight in turbulent combustion process [9,10]. As is described above, the description of heat release rates or flame front topology using CH concentration had been attempted widely.

Since the heat release rate also plays important roles in the sound generation mechanism in turbulence combustion field [11], CH PLIF measurement may provide the information about spatial and temporal fluctuations of sound source as well as the heat release rate. To understand these spatial and temporal fluctu-

* Corresponding author. Tel.: +82 51 510 2476; fax: +82 51 512 5236.
E-mail addresses: choigm@pusan.ac.kr (G.-M. Choi), yangjs@pusan.ac.kr (J.-S. Yang), djkim@pusan.ac.kr (D.-J. Kim), mtanahas@mes.titech.ac.jp (M. Tanahashi), tmiyauch@mes.titech.ac.jp (T. Miyauchi).
[1] Tel.: +82 51 510 3239; fax: +82 51 512 5236.
[2] Tel.: +82 51 510 2316; fax: +82 51 512 5236.
[3] Tel.: +81 3 5734 3181; fax: +81 3 5734 3181.
[4] Tel.: +81 3 5734 3183; fax: +81 3 5734 3183.

0040-6031/$ – see front matter © 2006 Elsevier B.V. All rights reserved.
doi:10.1016/j.tca.2006.11.017

ations in the combustor is very important for the development of the control scheme of turbulent combustion. In turbulent flames, heat release rate fluctuates spatially along the flame front since the local flame structure significantly affected by turbulence in the unburned gas. Although the chemical reaction rate is quite faster than convection, it is expected that the interaction between fluid dynamics and chemical reaction in the turbulent flames might differ from that in the laminar flames. In addition, CH fluorescence measurement has been applied to diffusion flame [2,3,5] or low pressure premixed flame [12] even though practical combustion systems are operated at atmospheric. Therefore, it is not clear whether CH PLIF is applicable to the estimation of local heat release rate in the lean premixed flame. Since CH–OH boundary has been used as a useful marker of the instantaneous reaction zone, the simultaneous measurement of CH and OH may promises better information of the instantaneous reaction zone even in lean conditions.

In present study, our objective is to measure the spatial fluctuation of heat release rate in the lean turbulent flame. Therefore, we investigate the relationship between the local heat release rate and CH concentration in the one-dimensional premixed flame and in intense turbulent premixed flame by numerical simulation. And then, we demonstrate the simultaneous CH and OH fluorescence measurements in the lean cellular flame as well as in laminar flames.

2. Numerical method and experimental conditions

In direct numerical simulation, we assumed that the external forces, Soret effect, Dufour effect, pressure gradient diffusion, bulk viscosity and radiative heat transfer could be negligible [13]. A methane–air reaction mechanism, which includes 279 elementary reactions (GRI mechanism) [14], is employed. The GRI mechanism includes 49 chemical species, so 48 sets of conservation equations for mass fraction are solved directly with mass, momentum and energy conservation equations. The thermal and transport properties of chemical species are calculated by CHEMKIN FORTRAN packages [15,16], where original programs are modified to be fully vectorized and parallelized.

The computational domain is selected to be 1.48 cm × 0.74 cm. Periodic boundary conditions are applied in the transverse (y) direction and Navier–Stokes Caracteristic Boundary Conditions (NSCBC) [17,18] is used in the streamwise (x) direction. A spectral method is used to discretize the governing equations in the transverse direction and a fourth order central finite difference scheme is used in the streamwise direction. Time integration is conducted by the 2nd-order Adams–Bashforth scheme. The computations are performed in 1409 × 512 grid points. Inflow boundary conditions for the chemical species are set equal to methane–air mixture with equivalent ratio of $\Phi = 0.6$ at 0.1 MPa and 298.15 K. Inflow turbulence is set to be $u'/S_L = 18.60$, and $l/\delta_L = 2.55$. Here, u' is rms of velocity fluctuation of turbulence, S_L is a laminar burning velocity that is determined by a preliminary one-dimensional premixed flame calculation, l is an integral length scale of turbulence, and δ_L is a laminar flame thickness. The turbulence at the inflow boundary is given by the preliminary calculation of two-dimensional homogeneous isotropic turbulence with a spectral method. The calculation of turbulence was conducted with periodic boundary conditions. The result at 1.5 eddy turnover time is used for the inflow boundary. After 1.5 eddy turnover time, the turbulent velocity field attained a fully developed state.

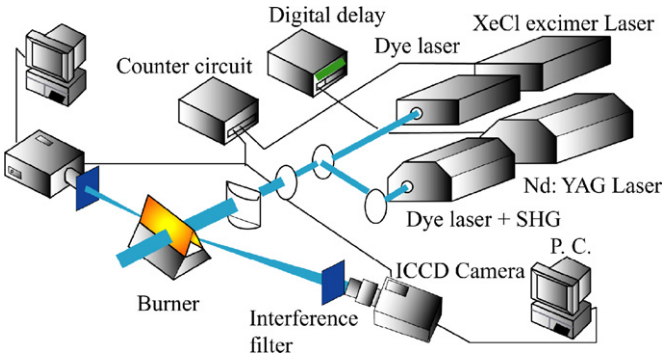

Fig. 1. Schematic diagram of the simultaneous CH and OH PLIF experiment.

The schematic diagram of the experimental setup for simultaneous CH and OH PLIF measurement is shown in Fig. 1. For CH-PLIF measurement, the Q_1 (7, 5) transition of the $B^2\Sigma^- – X^2\Pi(0, 0)$ band at 390.30 nm was excited and fluorescence from the A–X(1, 1), (0, 0) and B–X(0, 1) bands between 420 and 440 nm was detected [19,20]. Many groups have conducted successful CH PLIF measurements using this transition [10,21]. The laser system consists of a XeCl excimer laser (Lambda Phisik, LPX 110I, 308 nm, 200 mJ/pulse) and a dye laser (Lambda Phisik, Scanmate 2), and generates laser pulses with about 23–25 mJ/pulse. The XeCl excimer pumped dye laser system with BiBuQ dye in *p*-dioxane solvent, of which pulse width is 10–20 ns. The collection optics was located perpendicular to the laser sheet. An intensified CCD camera (Andor Technology, DH734-25U-03) with 105 mm F4.5 UV lens was used for the imaging. In order to block the flame radiation, 3 mm thick interference filter (KV-418 Scott) was used. To optimize signal-to-noise ratio, all measurements were conducted with an image intensifier gate time of 30 ns; this value was determined by preliminary experiments with a different gate time.

For OH PLIF measurement, the laser system consists of an Nd-YAG laser (Spectra-Physics, Quanta Ray PRO-110, 532 nm, 350 mJ/pulse) and a dye laser (Sirah Precisionscan), and generates laser pulses about 5 mJ/pulse. The Nd-YAG laser pumped dye laser system at 282.93 nm with Rhodamine 590 dye in methanol solvent, of which pulse width is 8–12 ns. The fluorescence from the A–X(1, 0) and (0, 0) bands (λ = 306–320 nm) was collected with a UV–Nikkor 105 mm/f4.5 lens and imaged onto a second intensified CCD camera (PI-MAX, 512RB-G1). This camera, which is located on the opposite side of the burner from the intensified CCD camera for CH, was fitted with WG305 and UG-11 interference filters to reject incident light. Temporal separation of the CH and OH probe lasers was set to within 150 ns.

In general, a rate equation can be formulated for the number of collected photons, N_p, within the detector integration time at

each pixel point [22]:

$$N_p = \zeta(\Omega/4\pi)V_c n_0 \left(\frac{B_{12}I_\nu}{c}\right) b_{12}\tau_1 A_{21}\left[t_0 + \tau_2 \exp\left(\frac{-t_0}{\tau_2}\right)\right],$$

where ζ is the optical transmission efficiency, Ω the collection solid angle, V_c the focal volume imaged by the corresponding pixel, n_0 the species number density in that volume, B_{12} the Einstein absorption coefficient between levels of the transition, I_ν the laser spectral intensity, c the light speed, τ_1 the response time to reach steady-state after the laser beam input, A_{21} the Einstein spontaneous emission coefficient between the levels of the transition, t_0 the laser pulse duration and τ_2 is the fall time for fluorescence decay after the excitation. For the case $t_0 \gg \tau_2$, quenching term will drop out. For that case, species number density is directly related to the measured signals. Since a τ_2 of shorter than 10 ns is estimated for present study condition, the measured CH fluorescence intensity is proportional to CH concentration to some extent.

The experiments were performed in a slot burner and flat burner (McKenna). For the slot burner, mixture of methane and air was supplied into the burner. The equivalence was changed between 0.8 and 1.2. The flow rate was 20.679 *l*/min. To measure CH and OH fluorescence intensity in the cellular lean premixed flame, we used a flat burner. With increasing flow rate for $0.6 < \Phi < 0.7$, cellular flame was formed on the flat burner. The flow rate was set to 50.0 *l*/min. Laser sheets for the slot burner and flat burner were approximately 8 mm.

3. Results and discussion

3.1. Heat release rate and CH radical concentration

Local heat release rate is one of the most interesting properties in the experimental study of unsteady reacting flows. The direct measure of burning rate or heat release rate has not been developed yet. Relationships between the local heat release rate and CH concentration are investigated by numerical simulations of methane–air premixed flames. Fig. 2 shows the distance between peaks of the heat release rate and CH mole fraction in one-dimensional laminar methane–air premixed flames. Numerical simulations are conducted by using PREMIX in CHEMKIN. As for a kinetic mechanism, GRI mechanism ver.2.11 is used. The mixture of methane and air is set to 0.1 MPa and 298.15 K. The distance between the peaks shows the minimum value of 35 μm for $\Phi = 0.9$ condition. For $\Phi < 0.9$ and >0.9, the distance tend to increase, while it is 70 μm for $\Phi = 0.5$ and 91 μm for $\Phi = 1.3$. These phenomena are ascribed to thickened reaction zone due to the reduction of burning rate. Considering that the flame thickness is estimated as about 0.1 mm, these values are small. These results suggest that CH concentration is a good enough indicator of the local heat release rate in the laminar-premixed flame.

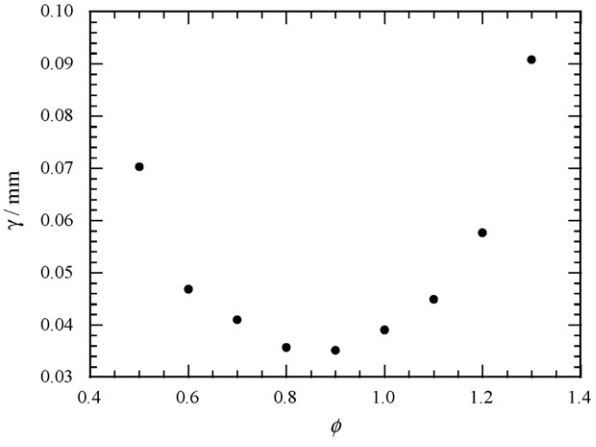

Fig. 2. Distance between peaks of the heat release rate and CH mole fraction (γ) in the laminar methane–air premixed flames.

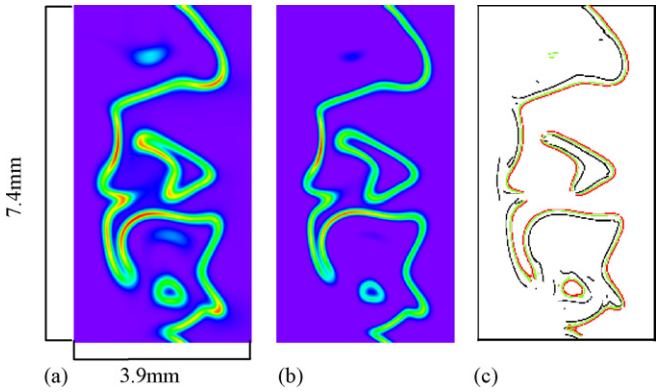

Fig. 3. Distributions of the heat release rate (a), CH mole fraction (b), and relation between peaks of the heat release rate and CH mole fraction (c) in a turbulent methane–air premixed flame. In (c), red; heat release rate, green; X_{CH} and black; flame fronts. (For interpretation of the references to colour in this figure legend, the reader is referred to the Web version of the article.)

Many results from PLIF [8,9,23] caution that at higher turbulence levels any relation between intermediate species and total reaction may breakdown as a result of localized flame quenching. Therefore, the relation between the local heat release rate and CH concentration in the turbulent flame is investigated by two-dimensional DNS of a methane–air turbulent premixed flame with a detailed kinetic mechanism. The distributions of the local heat release rate and CH mole fraction in the methane–air turbulent premixed flame obtained by DNS are shown in Fig. 3(a) and (b). Even for the premixed flame in high intensity turbulence, the distribution of the heat release rate coincides with that of CH mole fraction. In Fig. 3(c), the flame front (black lines), which is defined by the local maximum temperature gradient, is plotted with local maximum lines of heat release rate (red lines) and the CH mole fraction (green lines). Behind the preheat zone, the local maximum line of the heat release rate exists, and the local maximum line of CH radical is located just after that of the heat release rate. The two local maximum lines are nearly parallel and the distance between them is sustained to be nearly that of the corresponding laminar premixed flame. These results show that CH concentration is a good indicator of the heat release rate even in the intense turbulent premixed flames.

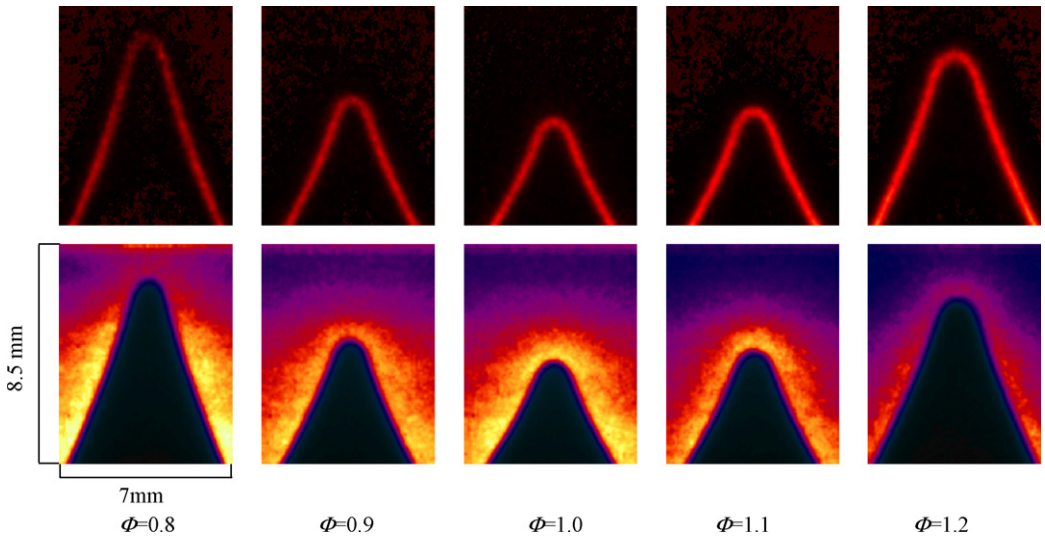

Fig. 4. CH (upper) and OH (lower) fluorescence images for methane–air premixed flames as a function of equivalence ratio in a slot burner.

3.2. Fundamental aspects of CH planar laser-induced fluorescence measurements

Fig. 4 shows the simultaneous CH and OH PLIF images for different equivalence ratio in the slot burner. An hundred images are averaged for each condition. CH fluorescence coincides with blue flame observed in direct photographs for each condition, while OH fluorescence shows high intensity in the fuel-lean region. The OH fluorescence region distributes wider than CH fluorescence. OH images represent that OH radical is a long-life intermediate of combustion. OH radicals are mostly present in hot combustion products and, to that extent, is an indicator of elevated temperature [24]. Thus, images of OH also show the boundary of the hot products with the cold reactants. On the other hand, CH images represent the distribution of a very short-life combustion intermediate that can be interpreted as the primary flame front. For all range of equivalence ratio measured in this study, CH fluorescence can be captured clearly and the intensity of CH fluorescence depends on the equivalence ratio. It should be noted that $\Phi = 0.8$ is the nearly the lower limit of the flammable range in the slot burner used in this study. From the simultaneous images of CH and OH fluorescence, we can observe that CH fluorescence distributions represent the primary reaction zone in present work condition. Therefore, relationship between local heat release rate and CH fluorescence intensity is expected.

In Fig. 5, the maximum intensity of CH fluorescence obtained by PLIF measurements are compared with the maximum CH mole fraction obtained by numerical simulations of the laminar flame with GRI mechanism ver. 2.11. CH mole fractions and fluorescence intensities are normalized by the value at $\Phi = 1.0$. The trend of the CH fluorescence intensity shows good agreement with that of CH mole fraction computed with GRI mechanism even though some qualitative discrepancies are observed in the lean and rich conditions. Though these discrepancies are ascribed to quenching process or temperature effect on species number density that exists on exciting level, etc., the reliable

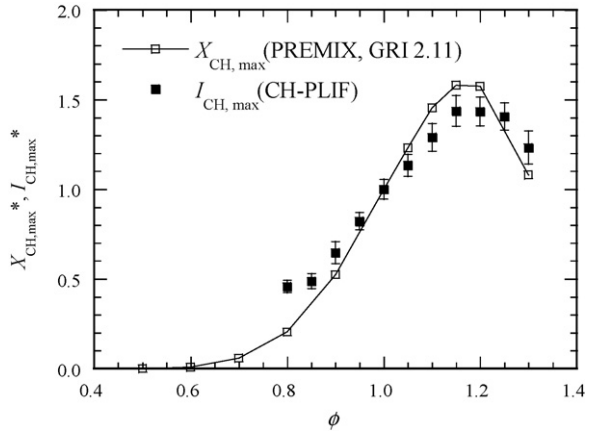

Fig. 5. CH mole fraction obtained by numerical simulations of one-dimensional laminar flame with GRI 2.11 and CH fluorescence intensity by CH PLIF.

reason is not elucidated in present work. Regardless of these discrepancies, CH PLIF intensity can represent the change of CH mole fraction due to the alteration of equivalence ratio.

To estimate the distribution of heat release rate using CH PLIF measurements in the turbulent combustion field, it is required

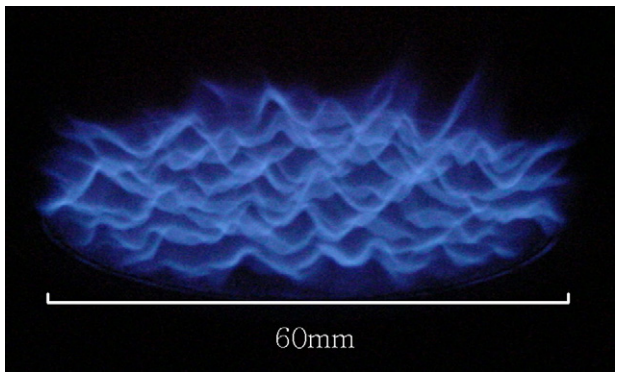

Fig. 6. Direct photograph of the cellular flame in a flat burner ($\Phi = 0.7$).

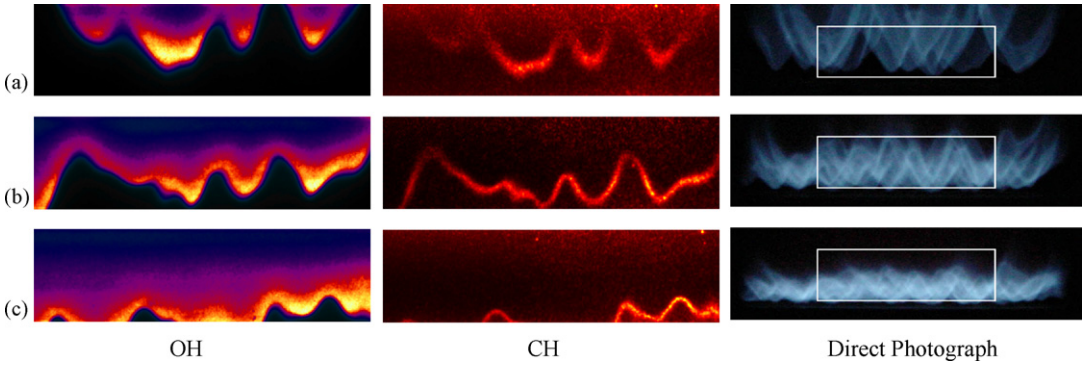

Fig. 7. OH (left hand side) and CH (middle) fluorescence images and direct photographs (right hand side) of the unstable cellular flames on a flat burner. (a) $\Phi = 0.60$, (b) $\Phi = 0.65$, (c) $\Phi = 0.70$, where white boxes (30 mm (W) × 8 mm (H)) in the direct photographs indicate the displayed regions in PLIF images.

to capture the spatial fluctuation of CH fluorescence intensity. Especially, because the CH concentration decreases significantly in the lean combusting condition, the establishment of CH PLIF in the lean condition is necessary. With the increase of the flow rate, the flame formed on a flat burner becomes unstable for lean conditions and shows cellular structure as shown in Fig. 6. The flame attaches on the sintered metal locally, and the local flame front thickness seems to change spatially. Simultaneous CH and OH PLIF measurements are conducted for the cellular flame in the flat burner for $0.6 < \Phi < 0.70$.

Fig. 7 shows the simultaneous CH and OH fluorescence images and corresponding direct photographs. White boxes in direct photographs represent the displayed region in the CH and OH fluorescence images. The height of the fluorescence image is about 8 mm. The direct photographs show that the flame front has three-dimensional structure and locally detaches from the burner surface with the decrease of equivalence ratio. Flame thickness seems to be thin and the flame front extended to downstream with decreasing equivalence ratio due to reduction of burning rate. The CH and OH fluorescence distributions represent this phenomenon very well. The CH fluorescence distributions agree with visualized flame front by direct photographs and OH radicals represent boundary of the hot products boundary with cold reactants. OH fluorescence images are visualized clearly compared to CH. Even for the lean condition, in which CH mole fraction significantly decreases compared to that in stoichiometric condition, the CH fluorescence can be measured. These results imply that CH PLIF measurements can be applicable for the estimation of the heat release fluctuations in the turbulent premixed flame. However, there are low intensity regions of CH fluorescence. Especially, these breakdown phenomena are observed obviously in the lean condition. These phenomena are ascribed to weak CH concentration or CH breakdown due to flame quenching. The reason is not clear at this stage. Additional investigation of PLIF measurement is necessary to provide more reliable information about heat release rate in the turbulent combustion.

4. Conclusion

Relationships between the local heat release rate and CH concentration are investigated by numerical simulations of methane–air premixed flames. Simultaneous CH and OH PLIF measurements are also conducted for lean cellular premixed flame as well as laminar flames. Effectiveness of CH PLIF measurement as for an indicator of the local heat release rate is demonstrated by comparison of CH PLIF experiments and numerical simulations including DNS with a detailed kinetic mechanism. From the results of DNS, even for the premixed flame in high intensity turbulence, the distribution of the local heat release rate coincides with that of CH mole fraction. From simultaneous measurement of CH PLIF in the slot burner, it is shown that CH PLIF intensity can represent difference of CH mole fraction due to the equivalence ratio. CH PLIF measurements are conducted for the cellular flames in the flat burner for $0.6 < \Phi < 0.70$. Even for lean condition, in which CH mole fraction significantly decreases compared with that in $\Phi = 1.0$, CH fluorescence can be measured. The results in the present study imply that CH PLIF measurements can be applicable for the estimation of the local heat release fluctuations in the turbulent premixed flame.

References

[1] M.J. Dyer, D.R. Crosley, Proc. Int. Conf. On Laser 84 (1985) 211–218.
[2] R.K. Hanson, Proc. Combust. Inst. 21 (1986) 1677–1691.
[3] J.M. Donbar, J.F. Driscoll, C.D. Carter, Combust. Flame 122 (2000) 1–19.
[4] M.W. Renfro, G.B. King, M. Laurendeau, Combust. Flame 122 (2000) 139–150.
[5] S.H. Starner, R.W. Bilger, R.W. Dibble, R.S. Barlow, D.C. Fourguette, M.B. Long, Proc. Combust. Inst. 24 (1992) 341–349.
[6] M.D. Smooke, Y. Xu, R.M. Zurn, P. Lin, J.H. Frank, M.B. Long, Proc. Combust. Inst. 24 (1992) 813–821.
[7] P.H. Paul, H.N. Najm, Proc. Combust. Inst. 27 (1998) 43–50.
[8] H.N. Najm, P.H. Paul, C.J. Mueller, P.S. Wyckoff, Combust. Flame 113 (1998) 312–332.
[9] P.H. Paul, J.E. Dec, Opt. Lett. 19 (1994) 998–1000.
[10] D. Han, M.G. Mungal, Proc. Combust. Inst. 28 (2000) 261–267.
[11] M. Tanahashi, T. Miyauchi, T.Y. Li, Smart Control of Turbulent Combustion, Springer-Verlag, Tokyo, 2001.
[12] P.A. Berg, D.A. Hill, A.R. Noble, G.P. Smith, J.B. Jaffries, D.R. Crosley, Combust. Flame 121 (2000) 223–235.
[13] T. Miyauchi, M. Tanahashi, K. Sasaki, T. Ozeki, Vortex-flame interaction in diffusion flames, Transport Phenomena in Combustion (Ed. C.H. Chen, Taylor & Francis, 1996) 1095–1105.
[14] http://www.euler.barkeley.edu/gri_mech/

[15] R.J. Kee, G. Dixon-Lewis, J. Warnatz, M.E. Coltrin, J.A. Miller, A Fortran computer code package for the evaluation of gas-phase multicomponent transport properties, SAND86-8246 (1986).
[16] R.J. Kee, F.M. Rupley, J.A. Miller, Chemkin-II: Fortran chemical kinetics packages for the analysis of gas phase chemical kinetics, SAND89-8009B (1989).
[17] T.J. Poinsot, S.K. Lele, J. Comput. Phys. 101 (1992) 104–129.
[18] M. Baum, T. Poinsot, D. Thevenin, J. Comput. Phys. 116 (1994) 247–261.
[19] C.D. Carter, J.M. Donbar, J.F. Driscoll, Appl. Phys. B 66 (1998) 129–132.
[20] N.L. Garland, D.R. Crosley, Appl. Opt. 24 (1985) 4229–4237.
[21] K.A. Watson, K.M. Lyons, J.M. Donbar, C.D. Carter, Combust. Flame 123 (2000) 252–265.
[22] Y.C. Chen, M.S. Mansour, Appl. Phys. B 64 (1997) 599–605.
[23] J.M. Samaniego, F.N. Egolfopoulos, C.T. Bowman, Combust. Sci. Technol. 109 (1995) 183–203.
[24] Q.-V. Nguyen, P.H. Paul, Proc. Combust. Inst. 26 (1996) 357–364.